Predicting gaps and overlaps in automated fiber placement composites by measuring sources of manufacturing process variations

Pantoji, S.A.; Kassapoglou, C.; Peeters, D.M.J.

DOI
10.1016/j.compositesb.2024.111891

Publication date
2024

Document Version
Final published version

Published in
Composites Part B: Engineering

Citation (APA)
Pantoji, S. A., Kassapoglou, C., & Peeters, D. M. J. (2024). Predicting gaps and overlaps in automated fiber placement composites by measuring sources of manufacturing process variations. *Composites Part B: Engineering*, *291*, Article 111891. https://doi.org/10.1016/j.compositesb.2024.111891

Composites Part B 291 (2025) 111891

Contents lists available at ScienceDirect

Composites Part B

journal homepage: www.elsevier.com/locate/composites

Predicting gaps and overlaps in Automated Fiber Placement composites by measuring sources of manufacturing process variations

Siddharth Pantoji [a], Christos Kassapoglou [a], Daniël Peeters [a,b,*]

[a] Faculty of Aerospace Engineering, Delft University of Technology, Kluyverweg 1, 2629 HS Delft, The Netherlands
[b] SAM XL - Smart Advanced Manufacturing, Rotterdamseweg 382c, 2629 HG Delft, The Netherlands

ARTICLE INFO

Dataset link: 4TU.ResearchData

Keywords:
Automated Fiber Placement
Gap and overlap defects

ABSTRACT

Manufacturing variations in the Automated Fiber Placement (AFP) process are one of the causes of gaps and overlaps. These manufacturing variations can be due to robot inaccuracy, tow lateral movement on the roller, tow width variation or tow compaction. An experimental setup was built to measure and investigate these various sources of manufacturing variations and their relative contributions to gap and overlap defects. This setup consisted of a commercial AFP head instrumented with additional sensors. Among all the measured sources of variations, lateral movement of the tow on the compaction roller was the biggest contributor to gaps and overlaps. The distributions of these sources of variations were fit with probability density functions. Random samples from these fits were used to simulate adjacent tows and predict the occurrence of gap and overlap defects. The distribution of predicted gaps correlated closely with the distribution of experimentally measured gaps. Thus, this approach of using statistical information about the sources of manufacturing variations to predict the frequency and magnitude of defects in a layup was validated.

1. Introduction

Most of the latest generation of regional jets, narrow-body, and wide-body jet airliners have composite parts manufactured using Automated Fibre Placement (AFP) [1–3]. AFP is a suitable, commonly used process for large composite part production and is expected to continue to be so. Huge backlogs in airliner orders translate to a need for faster manufacturing of these AFP composites. The runtime fraction of an AFP cell should be maximized to ensure high production rates.

However, utilization time fractions of AFP cells show that inspection and rework take up ~32% of the time [4]. This wastage of cell time is strongly linked to various types of AFP defects like gaps/overlaps, puckers, wrinkles, bridging, folds, twisted tows, missing tows, splices, fuzz balls etc. Gaps and overlaps are the most common of all these AFP defects. For example, they were found to be more than 57% of all the defects for a representative helicopter part [5]. For typical aerospace AFP composites, there is an allowable magnitude of gaps and overlaps. During the layup, every ply is inspected for defects. If a gap/overlap defect bigger than the allowable is found, it is reworked manually. This reduces the run time of the AFP cell.

For thermoset AFP composites, gap defects occurring during the layup are filled up to varying extents by percolation and squeeze flow due to lower matrix viscosity and the time and pressure seen in typical autoclave cycles [6]. It is an industry norm to lay thermoset tow material with a deliberate gap [7]. This is to avoid overlaps and the associated mechanical knockdowns due to waviness of the layup in the vicinity of the overlap. These deliberate gaps lead to non-uniform fiber volume fractions [8,9].

For thermoplastic AFP composites which are to be consolidated in situ, the gaps and overlaps occurring during layup would remain as-is. Thus, gap and overlap defects would result in voids and fiber waviness [10]. These voids and fiber waviness result in deteriorated structural performance. The void percentage seen in in-situ consolidated (ISC) thermoplastic parts would therefore be a hurdle to certification if not below the conventional 1% mark.

Manufacturing process variations is one of the causes of scatter in the mechanical properties of aerospace composites. This scatter leads to a selection of more conservative values of A-basis allowables [11]. Thus, these manufacturing variations are linked to the overdesign of aerostructures leading to significant economic impact [12].

1.1. Causes of gaps and overlaps

An ideal mesostructure for any performance-oriented AFP composite would have the tow laid such that the part has spatially uniform fiber volume fraction and desired fiber orientation. This would result in better mechanical performance and less part-to-part variation. This

* Corresponding author at: Faculty of Aerospace Engineering, Delft University of Technology, Kluyverweg 1, 2629 HS Delft, The Netherlands.
E-mail address: D.M.J.Peeters@TUDelft.nl (D. Peeters).

https://doi.org/10.1016/j.compositesb.2024.111891
Received 13 June 2024; Received in revised form 26 September 2024; Accepted 13 October 2024
Available online 19 October 2024

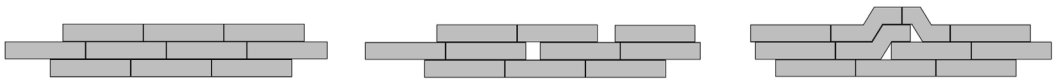

(a) Ideal (b) Gaps (c) Overlaps

Fig. 1. AFP layup cross section schematic. Ideal AFP composite mesostructure with abutting tows (a), gaps (b) and overlaps (c).

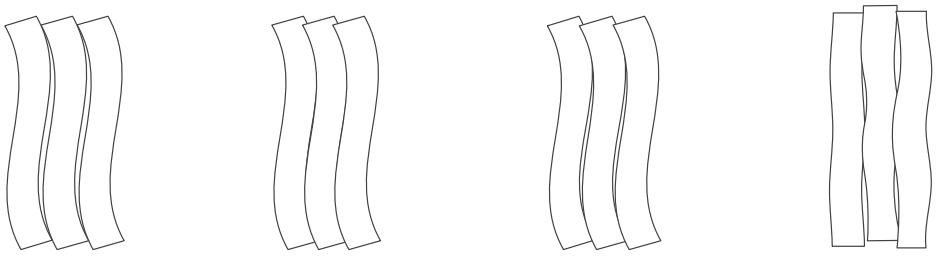

(a) Gaps (b) Overlaps (c) Gaps and overlaps (d) Gaps and overlaps

Fig. 2. AFP layup top view schematic. Gaps and overlaps due to shifting of tow path (a, b, c) and due to manufacturing process variations (d).

(a) Correct position and geometry (b) Position variation (c) Geometry variation

Fig. 3. AFP layup cross section schematic – ideal tow placement (a), tow placement with position variation (b), tow placement with geometry variation (c).

would require that the tow is laid beside each other and on top of other layers in an orderly and intimate fashion. This means that the tow edges are in abutting contact with the edges of the adjoining tow. Gaps are produced when the edges of adjacent tows do not touch each other whereas overlaps are produced when the edges cross over. This is illustrated in the schematics of Fig. 1.

1.2. The two major categories of gaps and overlaps

Gaps and overlaps can be classified according to their causes. Some gaps and overlaps occur due to an inherent limitation in tow path generation for parts that have tows laid in non-geodesic paths. This occurs in flat parts manufactured by fiber steering or in doubly curved parts due to their geometry. Tow paths are often generated by parallelly shifting a reference tow path. Depending on the amount of shift, the part has either gaps, overlaps or a combination of both at locations which can be predicted when the layup is designed before manufacturing starts. This is illustrated in the schematics of Fig. 2. Other gaps and overlaps occur due to manufacturing process variations. This class of gaps and overlaps are defects that occur due to incorrect relative placement of the edges of adjacent tows. This placement can have 2 reasons: one, variation in positioning of the tow and, two, variation in geometry of the tow. This is illustrated in the schematics of Fig. 3 where the blue colored rectangle denotes the section of a tow being laid on the substrate. Fig. 3(a) shows the ideal tow placement where the tow being laid is in intimate contact with the adjacent tow. Fig. 3(b) shows the laid tow which has correct geometry but is in the incorrect position. Fig. 3(c) shows the tow that has the correct position but has incorrect geometry.

Unlike gaps and overlaps occurring due to the shift of reference paths, the gaps and overlaps occurring due to manufacturing variations cannot be predicted before manufacturing. This means that it is not possible to know the frequency and magnitudes of defects that will occur in an AFP composite beforehand.

1.3. Gaps and overlaps due to manufacturing process variations

Fig. 4 shows the further breakdown of these manufacturing process variations into possible sources. Tow position variation could occur due to robot end effector inaccuracy and lateral movement of the tow on the roller. Tow geometry variations could occur due to tow width and thickness variation of the incoming tow or due to tow deformation while being compacted by the roller. The following paragraphs introduce the four major sources of manufacturing variations seen in AFP manufacturing.

Robot inaccuracy. AFP robots are programmed to lay down tow on a tool using computer-aided manufacturing (CAM) systems. The toolpath defined in the CAM systems is converted into a trajectory of the AFP head by the robot controller. The motion planning involves discretizing the defined toolpath into numerous linear segments, circular arcs or splines [13].

However, there is a difference in the planned toolpath and the achieved trajectory due to geometric, dynamic, thermal and system factors. Geometric factors include the inaccuracy of manufacturing of the manipulator parts and deflections due to loads like the AFP head weight and process forces. Therefore, the kinematic equations which relate the robot's joint space and cartesian space, do not do so perfectly. Such errors are expected to be higher in large envelope robotic cells, for example, those that make double aisle aircraft components. Dynamic factors like inertial loading and structural resonance can be significant for path-based control [14]. In many robotic applications, the end points of the motion need to be accurate. But for AFP systems, the path of the robot during laydown matters. Dynamic factors for an AFP head

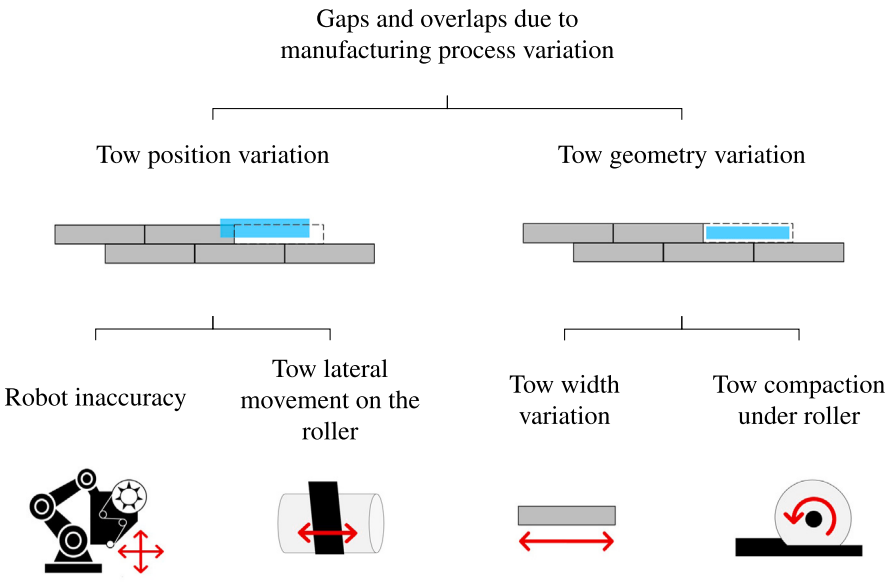

Fig. 4. Breakdown of the AFP manufacturing process variations which cause gap and overlap defects.

include the changing weight of the creels as the material is expended and reloaded. Another factor is inertial loading. Faster layup speeds are achieved by higher accelerations and decelerations in various phases of the layup cycle. However, this also reduces path accuracy.

Lateral movement of the tow on the roller. The tow feeding system of an AFP head moves tow from the spool to the compaction roller using a system of pulleys and chutes. During the start of each course, the tow is extended below the roller before it approaches the tool and presses against it. During this time, the tow may move sideways due to self-weight and residual stresses. The tow is under tension as it goes under the compaction roller during layup. This tow tension acts against the lateral movement of the tow. Steering can also move the tow sideways on the roller due to lateral tractions on the tow [15].

Tow width variation. AFP systems lay unidirectional tow material which is manufactured by slitting wider prepregs. However, the widths and thicknesses of slit tow can vary from the specified dimensions. As the adjacent tow is laid by the AFP head, less than specified width will cause a gap defect while more than specified width will cause an overlap defect. A tow twist will also lead to width variation causing gap defects.

Tow compaction. During the layup, a heat source raises the temperature of the tow while the compaction roller applies pressure. The heat flux and compaction force values depend on the tow material. For thermoset tows, the temperature should turn the tow tacky enough for it to stick to the substrate. For thermoplastic tows being laid with in situ consolidation, the temperature and pressure should be enough to ensure good ply to ply adhesion and to remove air. These process conditions cause the tow to reduce thickness and increase width. This deformation during layup is seen in higher magnitudes for thermoplastic tows as compared to thermoset tows [16,17].

In past work about these topics, various sensing techniques like laser line profilometry, optical coherence tomography (OCT) based profilometry, thermography and eddy current testing have been used on AFP heads to detect defects by sensing the tow while it is being laid. Thermography and eddy current techniques are better in detecting visually undetectable defects like loss of inter-ply adhesion. However, profilometry is most common due to its high profile rates and ability to robustly detect defects which change surface topography. [18–21].

Various experimental setups which looked at the tow before and after compaction were built previously for objectives such as: inline control of compaction force to affect width of the laid tow [22], online measurements of dry-fiber tow width variations to determine gap and overlap locations in the layup [23] demonstrating capability of inline control of process variables like compaction force, heating power and layup velocity [24]. Ghayoor et al. did full field DIC measurements of the compacted tow to understand deformations during AFP manufacturing [25]. Experiments by Uhart et al. show that even relatively small tool misalignments can lead to large changes in compaction forces. They developed an AFP head with hybrid position-force control to reduce the variation in compaction force in order to reduce gap and overlap defects while maintaining higher speeds [26]. Gonzalez Ojeda et al. looked at unwanted forces on the AFP head during layup on tools with complex corners and angles which in turn affects the accuracy of the layup process. They implemented a dynamic tool center point which updates according to a reduced order model of roller deformation behavior [27].

Accuracy of AFP robots has been measured and improved by using various techniques. Jeffries et al. have enhanced the accuracy of off-the-shelf manipulators by a secondary feedback loop using optical encoders [28]. Laser trackers have been used by various groups for reasons such as: increasing the accuracy of large envelope AFP robots by optimizing the kinematic parameters per positions and orientations along individual axes [29], plotting the repeatability at different speeds to find trade-offs in precision for increased production speeds [30], identifying and modeling geometric errors to upgrade kinematic models on gantry AFP machines [31], improving tooltip position accuracy by implementing a kinematic model calibrated to reduce variations due to deformation of the manipulator joints [32].

To the authors' knowledge, all these variations have not been measured simultaneously. There are existing setups which detect defects however, the individual contributions as well as the interactions of these variations to gaps and overlaps are not known. Moreover, tow lateral movement has never been measured.

The four aforementioned manufacturing variations occur concurrently and together determine the tow position and geometry deviations away from specified values. In turn, these tow positions and geometries determine the gaps and overlaps that occur in an AFP composite.

Our objective was to investigate the relative significance of these sources of manufacturing variations by building an experimental framework to measure them simultaneously. Once these individual contributions were known, we evaluated if it was possible to fit these

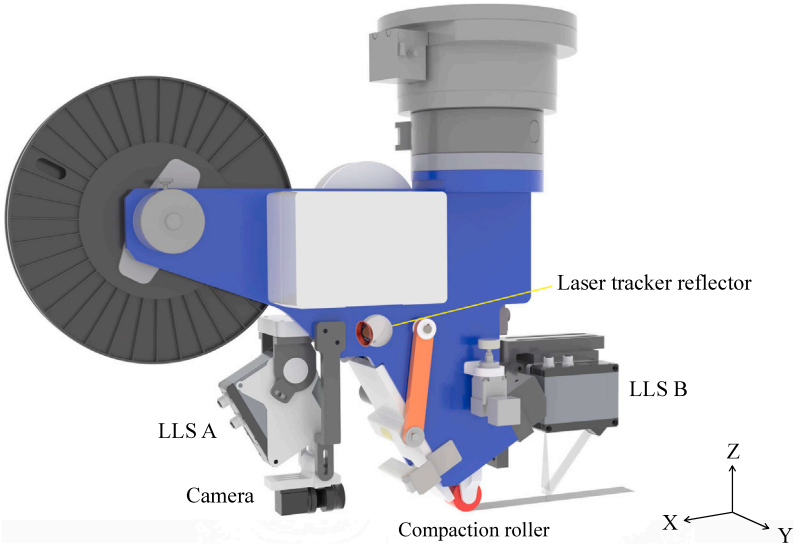

Fig. 5. CAD model showing various sensors setup on the AFP head. Layup is in the positive X direction.

distributions from a number of runs and then use them to predict the defects that would occur in the layup. This evaluation was done by comparing the predicted gaps with the experimentally measured gaps.

2. Experiment for measuring sources of manufacturing process variations

An experiment was designed to simultaneously measure the various sources of gap and overlap causing manufacturing variations during an AFP layup. These experiments were performed using an AFP machine at the robotic cell located at the TU Delft field lab – SAM XL (Smart Advanced Manufacturing XL).

2.1. Experimental setup overview

The measurement system consists of various sensors mounted on an AFP head as illustrated in Fig. 5. This system consists of an AFP-XS head made by ADD Composites as the end effector on a KUKA KR 210 R2700 robot manipulator. AFP-XS has a silicone compaction roller with a width of 31 mm and a diameter of 40 mm. The roller has a Shore hardness of 45 A. It has an infrared heater which increases the tack of the thermoset tow during layup. It can lay down tow with widths of 6.35 mm ($\frac{1}{4}$"), 12.7 mm ($\frac{1}{2}$") and 25.4 mm (1") [33]. The various sensors which make up the measuring system include a laser tracker - Leica AT960 MR, a camera - Ximea xiC USB 3.1 Gen1 MC050MG-SY-UB and two laser line scanners (LLS's) – (A) MicroEpilon 3060-25 & (B) MicroEpilon 3010-25. These are annotated in Fig. 5.

The laser tracker measures the position of the AFP head. The camera views the tow position as it goes under the compaction roller. LLS A measures the profile of the tow in the feed system before it reaches the compaction roller. LLS B measures the width of the tow after it has been laid.

Mounts for the camera and laser line scanner sensors required for this experiment were custom-designed and manufactured with PLA filament using fused filament fabrication. The mount geometry was designed to rigidly hold the sensors while allowing them to be moved and set in relation to the tow they are observing.

2.2. Layup procedure

The experiment involved laying down 6.35 mm wide unidirectional thermoset composite tow on a flat plate tool while recording tow position and tow geometry using the above-mentioned sensors. The prepreg tow was made from standard modulus carbon fiber with an epoxy matrix. The tool was a 1.5 m by 1 m rectangular steel plate which was clamp mounted on a measurement table. Note that it was not an aerospace grade flat tool. The 300 W IR heater was used at 80% power during layup.

31 straight lines of tow were laid. Each run was 1 m long. The maximum speed was set at 200 mm/s. The robot accelerated after the starting runway phase and decelerated for the stop at tow cutoff. It accelerated again at the end of the layup. Fig. 6 shows the program details of the layup along with the velocity profile. The tape tension was set at 6.7 N using a magnetic brake. The straight-line layups were programmed in the X-axis direction such that the Y co-ordinate will remain constant for each of them. The 31 tows had Y co-ordinates of 125 mm up to 500 mm with increments of 12.5 mm. To ensure compaction, the Z co-ordinates for the layup were set at −4 mm such that the tool center point (TCP) moves below the table surface which is at Z = 0. The compaction force was measured to be 377 N.

2.3. Data acquisition and analysis

The retroreflector required for the laser tracker measurements was magnetically attached to a mount/seat which was adhesively stuck to the frame of the AFP head. The laser tracker is a portable co-ordinate measuring machine (CMM) that uses a reflecting laser beam to measure the target's location and movement. The target is a retroreflector sphere with mirrors. The tracker model used for this experiment uses the Absolute Interferometer (AIFM) method. [34].

The Leica Tracker Pilot application was used to operate and record the position from the laser tracker every 10 ms. Each position data point was accompanied by a timestamp. The laser tracker has a typical accuracy of ±7 μm in distance measurement [35]. The AFP head positions recorded by the laser tracker were that of the achieved trajectory.

The difference of the achieved trajectory from the programmed path, in the Y direction, is calculated for each recorded set of position co-ordinates. For example, run 3 had a programmed Y co-ordinate of 150 during the layup. A recorded Y co-ordinate of 149.028 mm would mean a deviation of 0.972 mm for that data point.

The 5-megapixel monochrome optical camera was suitable because it is compact and lightweight. It has a 2464 x 2056 pixel CMOS sensor. It allows for a smaller region of interest to be specified from within the full 2464 x 2056 frame thus allowing for faster frame rates. The camera was paired with a lens that provides manual control on the focal length [36].

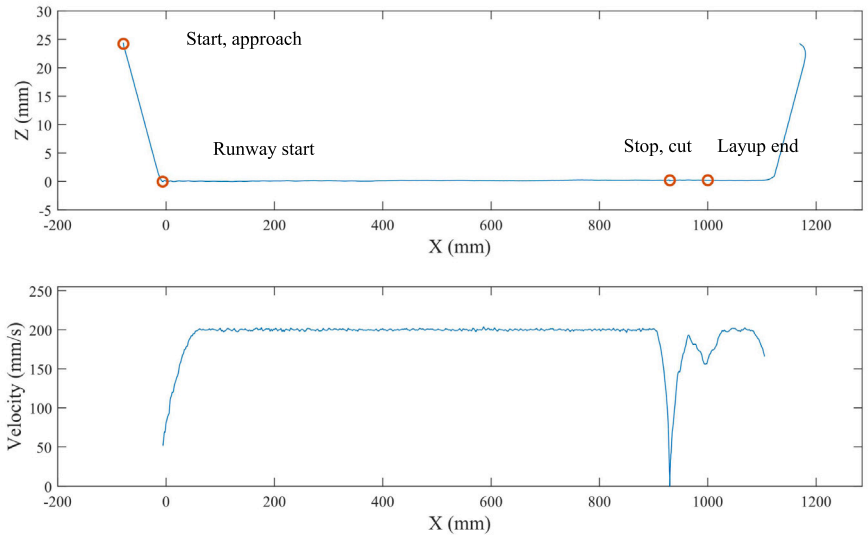

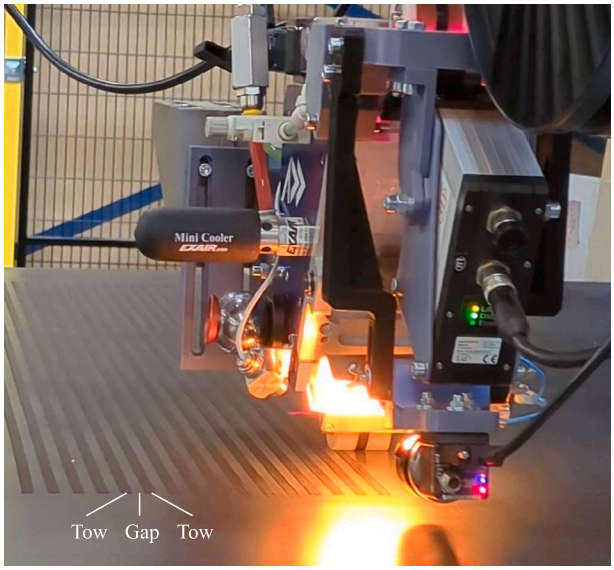

Fig. 6. AFP layup. Program details (top). Layup velocity profile (middle). Tow no 17 being laid (bottom).

The Ximea CamTool application was used to control and operate the camera. To maximize the frame rate, the camera data was acquired by operating it in a 'free-run' acquisition mode. The metadata from the application was used to get the timestamp for each frame.

The exposure time of the camera was set at 1 ms such that it captures an image that shows the black tow against the white roller with sufficient contrast. The mean frame rate was 62.5 Hz. Camera resolution in detecting the edge position of a tow was ~ 16 μm.

The tow position on the compaction roller was measured using image processing on each recorded frame. Fig. 7 shows an example frame with the measurement window. The center of the roller is annotated with a white dash-dotted line. Each frame is cropped to the window size and the average intensity of each column of pixels is calculated. The black tow has a much lower intensity than the white roller. Thus, the edge of the tow with respect to the dash-dotted center line is calculated by detecting this change in average intensity.

This value in pixels is converted to a metric measurement by using a pixel-to-mm length conversion scale. This scale is obtained from a reference image which has a checkerboard scale whose dimensions are accurately known from its micrograph. More details of this conversion scale calibration process can be found in Appendix B.

The LLSs are 2D profile sensors that were suitable because of their high profile resolution, high profile rate and proven past use in measuring composite tow dimensions [24,37]. These scanners reflect a line of laser light off the composite tow and use triangulation to measure the profile of the tow. The profile of the tow is output as Y, Z co-ordinates for each measuring point where Z is the measured height at position Y along the laser line. The width of the tow is along the Y axis, the thickness is along the Z axis while the length of the tow/layup direction is along the X axis. Both the LLSs have 2048 measurement points per profile. The measurement range for the sensors forms a symmetrical trapezoid with an average width of 25 mm in the tow width direction and a height of 15 mm in the tow thickness direction. Both sensors allow regions of interest to be defined to measure within fields smaller than the maximum available range to increase the profile rate [38].

The LLSs were operated using a Python API script. The exposure time of both the LLSs was set at 4 ms such that it reliably captures the tow profile in the minimum possible time. The mean profile rate

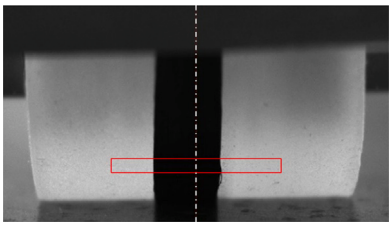

Fig. 7. Example frame recorded by the camera. A measurement window is annotated in red while the roller center is annotated with a white dash-dotted line.

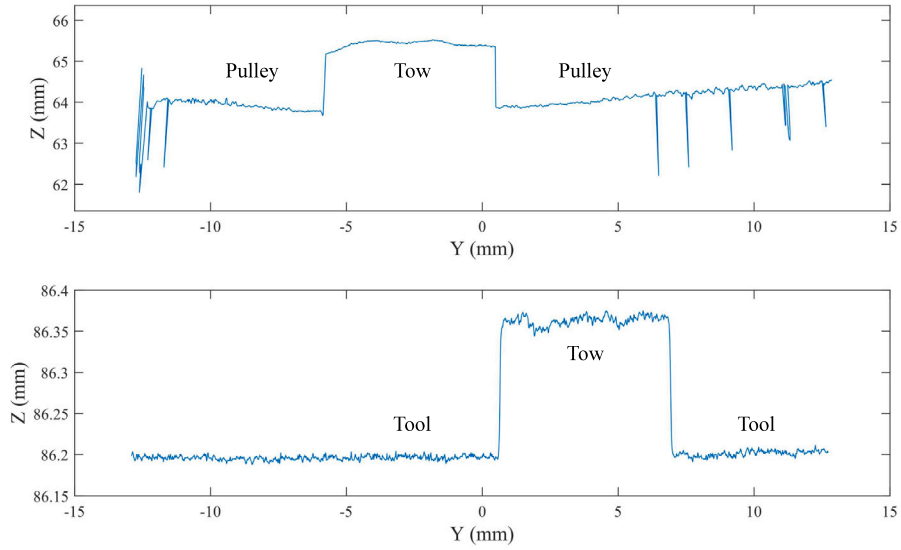

Fig. 8. Example profiles measured by LLS A (top) and LLS B (bottom).

was 83 Hz. The LLSs have a Y direction resolution of 12.2 μm and a Z direction resolution of 1.5 μm.

Fig. 8 shows example profiles from LLS A and LLS B. The tow edges are determined by detecting the sudden change in Z value. The exposure settings are selected to best view the tow. This means that objects like the feed system or the table in the view of the LLS can be overexposed. Some simple threshold filters are used to remove the anomalous points from each profile.

3. Relative significance of the sources of manufacturing process variations

Fig. 9 shows the distributions for the four measured variations - robot inaccuracy, tow lateral movement on the roller, tow width before compaction and tow width after compaction. The mean and standard deviation are marked in red at the bottom of each distribution. The distributions were obtained from measurements made during the layup of 31 tows where each tow was one meter long. As shown in Fig. 4, robot inaccuracy and lateral movement of the tow on the roller are causes of position variation while changes in tow width before and after compaction are causes of geometry variation.

Robot inaccuracy. Fig. 9(A) shows the distribution derived from position measurements of the AFP head from the laser tracker. The data from all tows was shifted to have the programmed path centered at 0 mm. Robot position variations have been calculated in the Y direction i.e. the tow width direction. These variations would therefore be an indicator of how the achieved trajectory differed from the programmed path.

The distribution has a mean value of −0.93 mm. The mean is not close to 0 mm, which implies that the position variations are not centered on the programmed path. This implies that the achieved trajectory got pushed to one side of the tool. This could be because of the undulation on the table surface or related to the pose of the robot when it is laying tow on the tool. The range of deviation was 0.54 mm which is 8.5% of the specified 6.35 mm tow width. Fig. 9(A) shows that a Logistic distribution can be used to statistically model the variation in the AFP head positions. The chosen distribution is for this particular AFP setup and program. Log-likelihood values were used to ensure a good fit.

The spread of the distribution may increase for robot manipulators with bigger work volumes, heavier AFP heads, faster layup speeds, higher accelerations and decelerations in programmed paths etc. The spread of the distribution will decrease for AFP setups which have increased path accuracy of robots due to various strategies such as additional feedback loops, improved kinematic models or robot cell specific compensation [28,29].

Lateral movement of the tow on the roller. Fig. 9(B) shows the distribution derived from the tow position measurements made from camera frames. The center of the tow is tracked while the tow is on the compaction roller. These position measurements were made with respect to the roller center line as shown in Fig. 7. This roller center position is also annotated in Fig. 9(B). The distribution is an indicator of how the tow moves laterally about its expected center position on the compaction roller.

The distribution has a mean of 0.29 mm which implies that the overall tow movement is shifted from the center of the roller. The range of deviation was 1.4 mm which is 22.1% of the specified 6.35 mm tow width. Fig. 9(B) shows that an Extreme Value distribution can be used to statistically model the variation in tow positions on the roller.

Of the four distributions for various sources of the variations, this distribution had the least samples. This is due to the frame rate limitations of the camera. It was observed that the tow was moving laterally

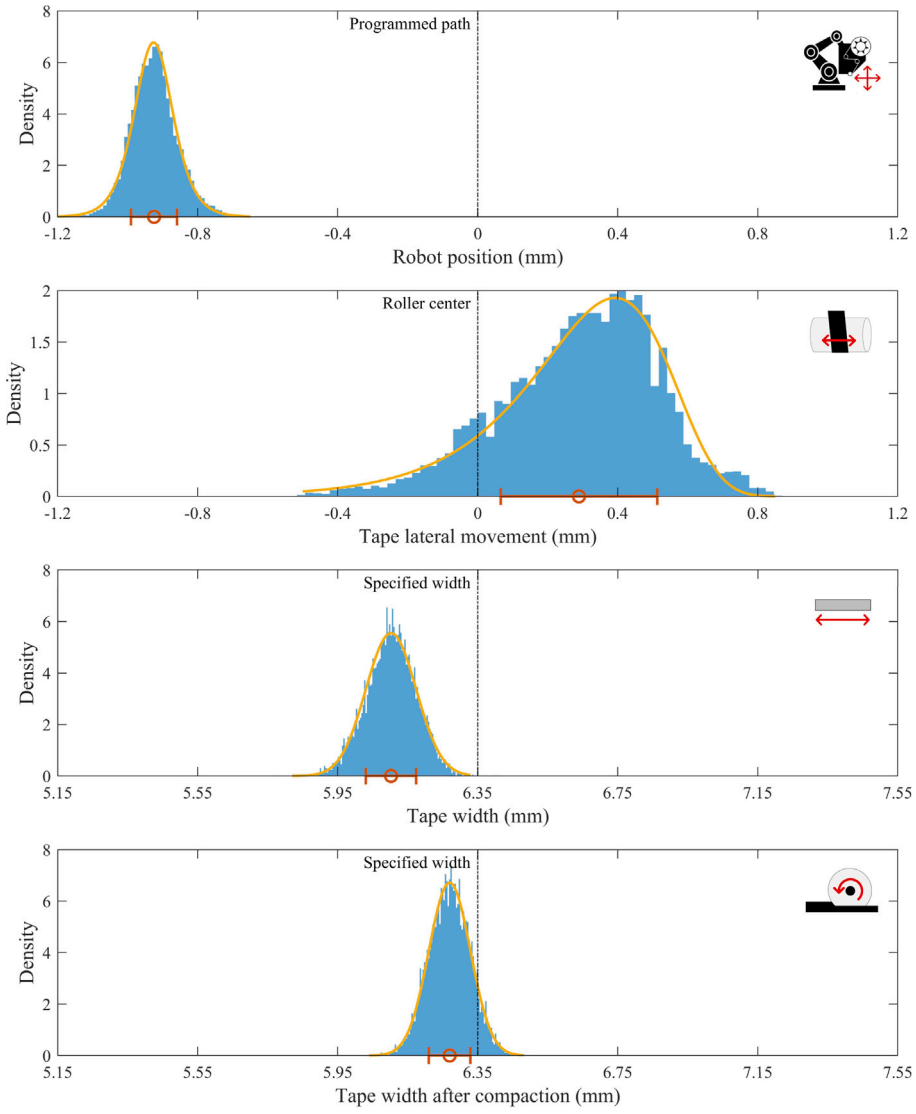

Fig. 9. A, B, C, D (top to bottom). Measured manufacturing variations that cause gaps and overlaps. Note that the X axis is equally scaled. Means and $\pm 1\sigma$ values are annotated in red. Distribution fits are annotated in yellow. (For interpretation of the references to color in this figure legend, the reader is referred to the web version of this article.)

Table 1
Summary of measured manufacturing variations which cause gaps and overlaps.

	Robot inaccuracy	Tow lateral movement	Tow width variation	Tow width variation after compaction
Distribution fit	Logistic	Extreme Value	Normal	Normal
Range (mm)	0.54	1.4	0.63	0.48
Range as percentage of specified width	8.5%	22.1%	9.9%	7.5%
Mean (mm)	−0.93	0.29	6.10	6.27
Standard deviation (mm)	0.07	0.22	0.07	0.06

on the pulleys in the feed system as well. It then passes through a rectangular metallic chute. This chute has a width clearance which reduces from 0.5 mm to 0 mm where the tow has minimal clearance to move. The tow then reaches the roller where it moves laterally as seen in the distribution plot.

During past experiments of the authors which used a pristine compaction roller, the distribution of tow lateral movement was centered almost exactly at the roller center line [39]. However, the present experiment used a compaction roller which was worn from significant earlier use. The wear and tear may have been asymmetrical due to the steering conditions during this earlier use.

The spread of this distribution is expected to be narrower for tackier materials and for higher tow tension arising from the spool brake. This is because the tractions in the width direction which cause lateral

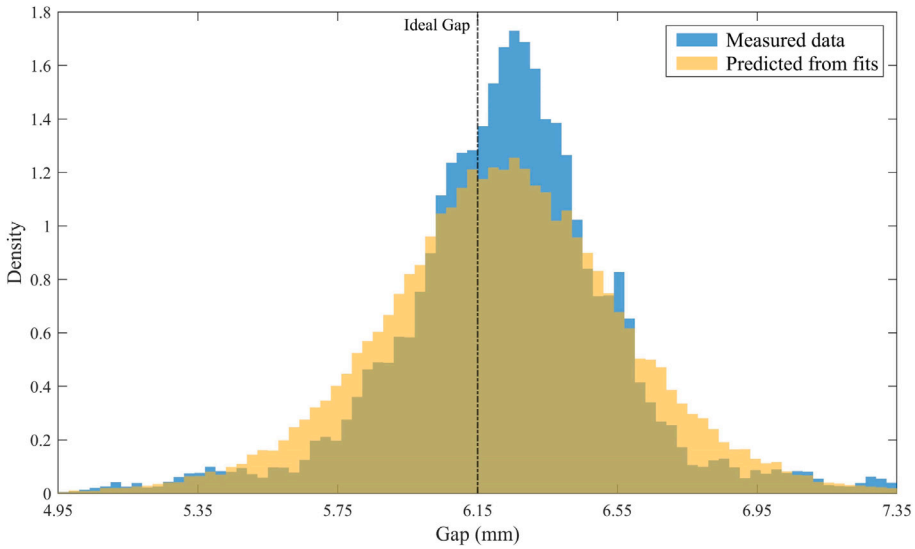

Fig. 10. Distribution of experimentally measured gaps overlayed with the distribution of predicted gaps.

Table 2
Comparison of measured gaps and predicted gaps.

	Measured gaps	Predicted gaps	Percent difference
Mean (mm)	6.24	6.23	0.16
Standard deviation (mm)	0.33	0.36	9.09
90th percentile (mm)	6.59	6.67	1.21
99th percentile (mm)	7.21	7.13	1.11

movements will be opposed by friction forces and a component of the tow tension.

Tow width variation. Fig. 9(C) shows the distribution derived from geometry measurements of the tow made with a laser line scanner. LLS A recorded profiles of the tow in the tow feed system before it enters the chute leading to the compaction roller. The tow width variation has been recorded by calculating the length of the top edge in each profile. The distribution is an indicator of how the width of the tow varies for the given batch of the unidirectional tow material.

The distribution has a mean of 6.10 mm and a standard deviation of 0.07. The mean value is less than the specified tow width of 6.35 mm. The range of deviation was 0.63 mm which is 9.9% of the specified 6.35 mm tow width. Fig. 9(C) shows that a Normal distribution can be used to statistically model the width of the tow.

The data indicates that the tow slitting process is quite well controlled for the used brand and specification of unidirectional tow. However, improvements can be made in the process to get the mean width to match the specified value and to reduce the overall spread. The tow raw material width is much less controlled for some other AFP materials like dry fiber tows used for resin infusion processes and for some newer material systems used for manufacturing ceramic matrix composites [23,40].

Some tow materials are specified to have unilateral tolerance only on the lower side of the specified width. For example, $6.35^{+0.0}_{-0.25}$ mm. Preventing overlaps in the layup is usually more important than preventing gaps. This is because overlaps will lead to waviness which is a worse outcome compared to gaps.

Tow compaction. Fig. 9(D) also shows the distribution derived from geometry measurements of the tow made with a laser line scanner. LLS B recorded profiles of the tow after it was laid on the tool. The tow width variation after compaction has been recorded by calculating the edge-to-edge distance in each measured profile.

The distribution is an indicator of how the width of the tow varies after it has been compacted by the compaction roller. The distribution has a mean of 6.27 mm and a standard deviation of 0.06. The range of deviation was 0.48 mm which is 7.5% of the specified 6.35 mm tow width. Fig. 9(D) shows that a Normal distribution can be used to statistically model the width of the tow after compaction.

Of the four measured sources of manufacturing variations, this source had the narrowest spread. For the thermoset material that was used in this experiment, the spread was slightly smaller than the spread for tow width before compaction. However, one can expect this spread to be much wider for thermoplastic materials. This can be due to the squeeze flow of the tow under the pressure of the compaction roller accompanied by tow spreading in the final sections of the feed system [17,22].

4. Prediction of the occurrence of gaps and overlaps

Fig. 9 shows the distributions for the four measured variations and the probability density functions which were fit to these four distributions. The distributions were obtained from measurements made during the layup of 31 tows. However, there may be thousands of such tows in an entire layup of a laminate. This section focuses on the hypothesis that the distribution fits from these few tows can be used to estimate the occurrence of gaps and overlaps in the entire layup. During a layup, gap and overlap defects in a certain lamina are expected to interact with similar defects in other adjacent laminae. These interactions will be neglected.

To predict gaps between two adjacent tows, many instances of the profile of these two tows were simulated. Each of these Monte Carlo tow simulations were done by randomly sampling from each of the four distribution fits. The algorithm used for this simulation can be found in Appendix A.

Thus one tow was simulated by using information from two position related samples and two geometry related samples. The adjacent tow

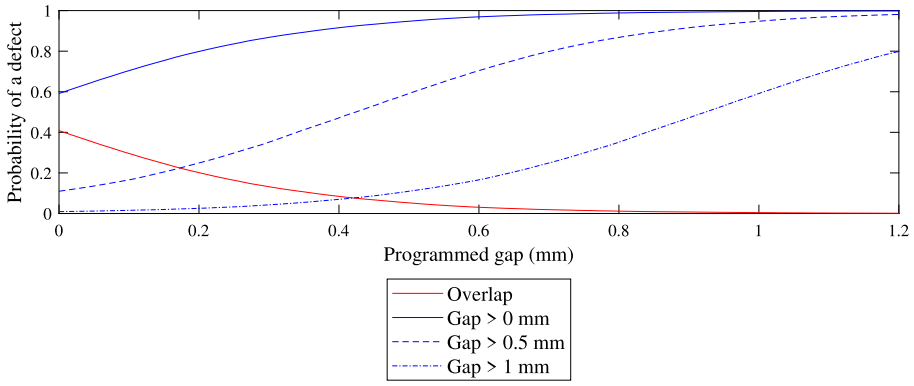

Fig. 11. Probability predictions of defects for various values of programmed gap between adjacent tows.

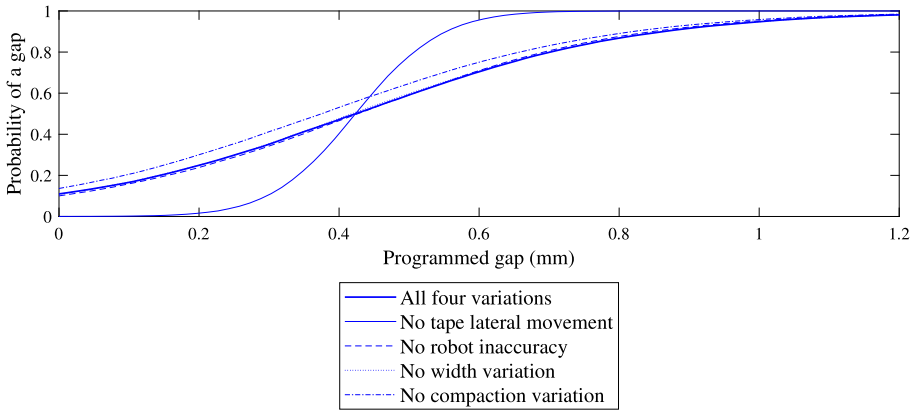

Fig. 12. Probability predictions of a gap (greater than 0.5 mm) when variations from each of the four sources of variations are eliminated one at a time.

was also simulated using the same algorithm starting with the programmed shift of 12.5 mm for adjacent tows. Now that two adjacent tows had been simulated, the gap in this simulated instance can be determined. These simulated gaps form the yellow colored distribution seen in Fig. 10. This is the prediction about the occurrence of gaps of various magnitudes.

The gaps in the layup done during the experiment were measured by traversing an LLS over the entire 1 m length of each pair of adjacently laid tow. There were 30 gaps in between 31 adjacent tows. The measured gaps form the blue distribution in Fig. 10.

The LLS made 46,384 observations during these scans. Hence the two adjacent tows were also simulated an equal number of times. It can be observed from Fig. 10 that the location of the distribution from predicted gaps aligns closely with the distribution of the measured gaps. This is also seen in the comparison of mean values in Table 2. This table also gives a comparison of the spread of the two distributions using standard deviation, 90th and 99th percentile values of defect magnitude. The closeness of values describing both the location and the spread validate this prediction technique. Since simulations use data from a trial experiment, it might be feasible to use this approach to reduce the effort spent in determining allowable defect magnitudes and frequencies.

Similar simulations can be carried out for various values of shift in adjacent tows which in turn decide the programmed gap between those adjacent tows. Fig. 11 shows the predictions for probability of gap and overlap defects occurring for various values of programmed gaps. The laminate can benefit structurally from reducing the programmed gap. The time spent in manufacturing steps like debulking, autoclave cycles or vacuum overbagging may also be reduced. However, reducing programmed gaps would result in more frequent overlap defects. The overlap defects would need to be repaired and AFP cell time would be wasted. It is thus possible to balance the aforementioned competing effects of programmed gap values and take informed decisions regarding them.

Fig. 12 gives an example of how the probability of defects can be related to the contribution of various sources of variation. Each of the thinner blue curves shows the trends in probability of a gap greater than 0.5 mm, if variations from one of the four sources are eliminated at a time. An example of the utility of such relationships is that it can inform us about how programmed gap values can be lowered if tow lateral movement is eliminated/minimized. This can help in the prioritizing of various process improvement efforts. These efforts may include adding secondary feedback to make robots more accurate, improving tow feed systems to reduce lateral movement of the tow, tighter width control in the tow slitting process or implementing layup path planning which accounts for tow width after compaction when determining the shift between tows.

Another significant relationship lies in the magnitude of the position variations and geometry variations and the magnitude of defects they both create. For the same magnitude of variation, position variations create defects twice in magnitude of defects created by geometry variations. For example, a 1 mm position variation leads to a 1 mm defect magnitude on both sides of the tow whereas a 1 mm width variation leads to a 0.5 mm defect magnitude on both sides of the tow.

Note that the probabilities mentioned earlier are that of finding a defect at a certain location of a layup. To convert these probabilities to representative example defect maps in a virtual layup, future work may look at dependent sampling methods along with some scheme which considers the distance between two instances of the simulation in the layup direction.

The predictions discussed earlier focused on results useful at the laminate level. The following paragraphs focus on results that would be useful at the individual tow level. Table 1 showed that tow lateral

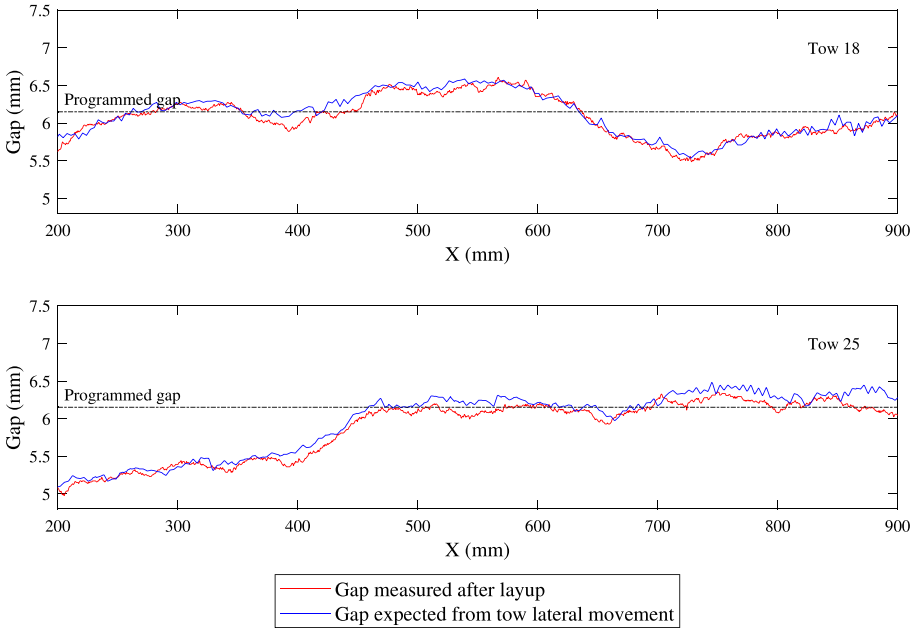

Fig. 13. An individual tow level comparison of the measured gaps with the gaps expected from the tow lateral movement. This example data is from tow 18 (and its adjacent tow 19) and tow 25 (and its adjacent tow 26) respectively.

movement was found to be the biggest contributor to gaps and overlaps. The following result proposes the utility of using the tow lateral movement data from the camera as feedback to the robot controller which can use it to compensate its path. This could lead to reductions in gap and overlap defects.

Fig. 13(top) shows the measured gap between tow 18 and tow 19, in red. These measurements were made by traversing an LLS over the laid tow. The gap can be seen deviating from the programmed gap of 6.15 mm. These deviations would lead to a higher number of defects. However, if the AFP robot detects these impending defects during layup, it can correct its position to compensate against them. Similar online corrections have been used to compensate against robot path inaccuracy and tow material width [22,28].

The tow lateral movement data along with the mean tow width were recorded during the layup of tow 18 and tow 19 and were used in determining the edges of the tow, thus leading to the expected gap along the layup. This expected gap is shown in blue in Fig. 13(top). The shown data has been appropriately shifted in the layup direction to align them. This was to correct the lag in the measured gap as compared to the tow lateral movement recorded on the compaction roller.

It can be seen from Fig. 13 that for both example runs, the gap expected from the camera data agrees closely with the measured gap data. A future AFP system could implement a feedback loop that uses this tow position information from the camera. The position detection and compensation calculation are not computationally expensive. Thus, future work can investigate if this approach could be used for online correction.

5. Summary & conclusions

An experimental setup involving various sensors mounted on an AFP head was implemented to simultaneously measure the sources of manufacturing variations in AFP composites. The measurements made during the layup revealed the relative significance of these sources. These measurements were used to successfully predict the occurrence of gaps and overlaps.

The experimental setup consisted of an AFP head instrumented with a laser tracker, a camera and laser line scanners. Each of these sensors measured a particular source of variation. The manufacturing variations were broken down into two categories depending on if they cause gaps and overlaps due to position variation or geometry variation. Robot inaccuracy and lateral movement of the tow on the roller are causes of position variation while changes in tow width and tow width after compaction are causes of geometry variation. The laser tracker measured robot accuracy. The camera measured tow lateral movement. The laser line scanners measured the width of the tow before and after compaction. Among all the measured sources of variations, lateral movement of the tow was the biggest contributor to gap/overlap causing deviations.

The four distributions obtained by measuring these sources of variations were fit with various probability density functions (PDFs). Random samples from these four distribution fits were used to simulate adjacent tows. The distribution of predicted gaps from these simulations was compared with the distribution of measured gaps. The location and spread of these distributions were in good agreement. Thus, statistical information from a trial experiment can be useful in predicting the magnitude and frequency of gap and overlap defects caused due to manufacturing variations in AFP composite laminates. At the individual tow level, the utility of the tow lateral movement data for online robot path compensation against anticipated defects has been proposed.

CRediT authorship contribution statement

Siddharth Pantoji: Writing – original draft, Visualization, Validation, Software, Methodology, Investigation, Formal analysis, Data curation, Conceptualization. **Christos Kassapoglou:** Writing – review & editing, Supervision, Project administration. **Daniël Peeters:** Writing – review & editing, Supervision, Resources, Project administration, Funding acquisition.

Declaration of competing interest

The authors declare that they have no known competing financial interests or personal relationships that could have appeared to influence the work reported in this paper.

Acknowledgments

The authors acknowledge the support of André Mendes Florindo in training for the use of the SAM XL AFP cell and Daniel Atherstone for the CAD modeling of the sensor mounts.

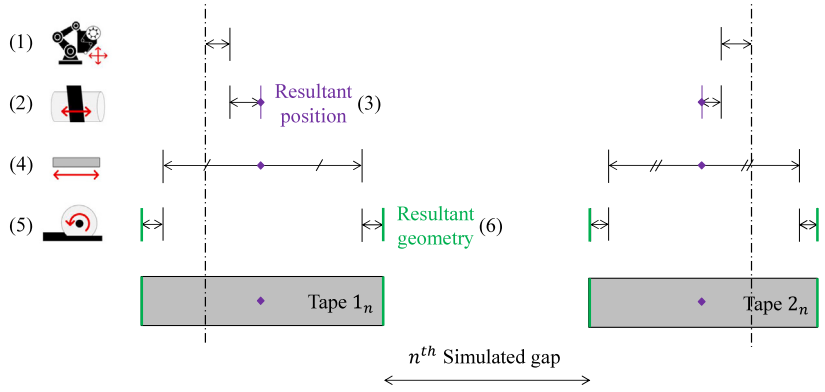

Fig. A.14. Schematic depicting the steps to simulate a tow section per the algorithm enumerated in this section. The dot-dashed lines represent the programmed tow-to-tow distance. Each double arrow line depicts a value drawn from a distribution fit. Two simulated adjacent tows and the resulting simulated gap is shown.

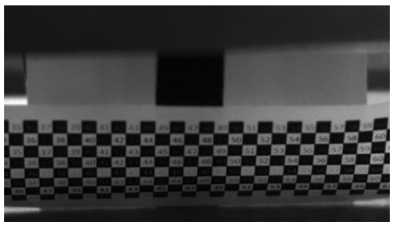

Fig. B.15. Example frame showing checkerboard scale.

Appendix A. Adjacent tape simulation algorithm

The algorithm to simulate a tow section was as follows:

1. A position value is sampled from the Logistic distribution in Fig. 9(A). This position value describes the position of the AFP head/robot.
2. This was followed by the sampling of another position value from the Extreme Value distribution seen in Fig. 9(B). This position value describes the position of the tow on the roller.
3. These two positions were added to get resultant tow position value. We now know the tow center position for this simulation.
4. This is followed by a tow width value sample from the Normal distribution in Fig. 9(C). Half of this tow width value is added and subtracted from the position value to get the left and right edges of the tow.
5. This was followed by sampling of a value of the width after compaction from the Normal distribution seen in Fig. 9(D). It was made sure that this sample had a value greater than the value of the initial width sampled earlier. If not resampling was done until this condition is satisfied.
6. The difference between the tow width after compaction and before compaction was used to pad the simulated tow width.

Fig. A.14 illustrates the steps in this algorithm by using a schematic.

Appendix B. Pixel-to-mm scale calibration

The pixel-to-mm scale calibration was carefully planned and executed in the following steps:

1. The camera frame and lens focus was adjusted to get a sharp view of the region of the tape in the measurement window (annotated in red) seen in Fig. 7. The selected lens is manufactured for applications in 2D/3D metrology and robotics vision.
2. The checkerboard scale was curved to match the curvature of the compaction roller and placed on it in different positions to capture several reference images. Fig. B.15 shows an example of an image with the checkerboard.
3. The calibration process used four reference images which were captured before the experiment and four which were captured after the experiment. This was to ensure that there was no change in the calibration value during the experiment due to camera mount movement due to the robot's motion.
4. The checkerboard scale is marked with numbers to make it easy to identify corners of particular squares. The distance between the corners of particular squares is compared between the micrograph and the reference images.
5. The earlier step was done eight times, once each for each of the eight reference images. Each reference image had different areas of the checkerboard in the measurement window. The average of these eight values was used for tape lateral movement calculations.

Data availability

Raw data from the mentioned experiment is available on the 4TU.ResearchData repository.

References

[1] Sloan J. Large, high-volume, infused composite structures on the aerospace horizon. CompositesWorld 2019. URL https://www.compositesworld.com/articles/large-high-volume-infused-composite-structures-on-the-aerospace-horizon.
[2] Sloan J. Evolving AFP for the next generation. CompositesWorld 2019. URL https://www.compositesworld.com/articles/evolving-afp-for-the-next-generation.
[3] Coriolis Composites. Coriolis industry references. 2024, URL https://www.coriolis-composites.com/references/industry/.
[4] Rudberg T, Nielson J, Henscheid M, Cemenska J. Improving AFP cell performance. SAE Int J Aerosp 2014;7(2):317–21. http://dx.doi.org/10.4271/2014-01-2272.
[5] Del Rossi D, Cadran V, Thakur P, Palardy-Sim M, Lapalme M, Lessard L. Experimental investigation of the effect of half gap/half overlap defects on the strength of composite structures fabricated using automated fibre placement (AFP). Composites A 2021;150(May):106610. http://dx.doi.org/10.1016/j.compositesa.2021.106610.
[6] Belnoue JP, Mesogitis T, Nixon-Pearson OJ, Kratz J, Ivanov DS, Partridge IK, Potter KD, Hallett SR. Understanding and predicting defect formation in automated fibre placement pre-preg laminates. Composites A 2017;102:196–206. http://dx.doi.org/10.1016/j.compositesa.2017.08.008.

[7] Lukaszewicz DH, Ward C, Potter KD. The engineering aspects of automated prepreg layup: History, present and future. Composites B 2012;43(3):997–1009. http://dx.doi.org/10.1016/j.compositesb.2011.12.003, URL http://dx.doi.org/10.1016/j.compositesb.2011.12.003.

[8] Guin WE, Jackson JR, Bosley CM. Effects of tow-to-tow gaps in composite laminates fabricated via automated fiber placement. Composites A 2018;115:66–75. http://dx.doi.org/10.1016/J.COMPOSITESA.2018.09.014.

[9] Ghayour M, Ganesan R, Hojjati M. Flexural response of composite beams made by Automated Fiber Placement process: Effect of fiber tow gaps. Composites B 2020;201(April):108368. http://dx.doi.org/10.1016/j.compositesb.2020.108368.

[10] Mayer M, Schuster A, Brandt L, Deden D, Fischer F. Integral quality assurance method for a CFRP aircraft fuselage skin: Gap and overlap measurement for thermoplastic AFP. In: Flexible automation and intelligent manufacturing (FIAM 2023). 2023, p. 525–34. http://dx.doi.org/10.1007/978-3-031-38241-3_59.

[11] Kassapoglou C. Design and analysis of composite structures. In: Design and analysis of composite structures. 2010, http://dx.doi.org/10.2514/4.867804.

[12] van Grootel A, Chang J, Wardle BL, Olivetti E. Manufacturing variability drives significant environmental and economic impact: The case of carbon fiber reinforced polymer composites in the aerospace industry. J Clean Prod 2020;261:121087. http://dx.doi.org/10.1016/j.jclepro.2020.121087.

[13] Mendes Florindo AM. LayLa: An open-source offine programming framework for com-posite deposition. 2020, URL https://repository.tudelft.nl/islandora/object/uuid:b13ad6e0-625a-42b1-bafb-1581ea31e20f?collection=education.

[14] Greenway B. Robot accurary. In: Industrial robot, vol. 27, (no. 4):Emerald Group Publishing Ltd.; 2000, p. 257–65. http://dx.doi.org/10.1108/01439910010372136.

[15] Rajan S, Sutton MA, Sockalingam S, McMakin W, Gurdal Z, Kidane A. Simulations and experiments for automated fiber placement of prepreg slit tape: Wrinkle formation and fundamental observations. Composites B 2020;201(January):108287. http://dx.doi.org/10.1016/j.compositesb.2020.108287.

[16] van Kollenburg J. The effects of local fibre steering. 2022, p. 3333–6, URL https://repository.tudelft.nl/islandora/object/uuid:ddfe7c0e-46d7-4a2f-95d2-72850c39a073?collection=education.

[17] Agarwal S. Width deformation of thermo- plastic prepreg tapes during in- situ Automated Fiber Placement. Delft University of Technology; 2023, URL https://repository.tudelft.nl/islandora/object/uuid:6b5f9a4c-7303-4b9d-9015-1d3772193138?collection=education.

[18] Juarez PD, Gregory ED. In situ thermal inspection of automated fiber placement for manufacturing induced defects. Composites B 2021;220(January):109002. http://dx.doi.org/10.1016/j.compositesb.2021.109002.

[19] Mussatayev M, Yi Q, Fitzgerald M, Maes VK, Wilcox P, Hughes R. Directional eddy current probe configuration for in-line detection of out-of-plane wrinkles. Composites B 2024;268(August 2023):111048. http://dx.doi.org/10.1016/j.compositesb.2023.111048.

[20] Rivard M, Palardy-Sim M, Lamouche G, Roy S, Padioleau C, Beauchesne A, Levesque D, Boismenu F, Dicaire LG, Boisvert J, Peters S, Chen J, Octeau MA, Robles JB, Ferland F, Tanguay M, Hissett J, Swope D, Albers S, Harper R, Wright K, Buhrkuhl B, Klakken M, Lund G, Yousefpour A. Enabling responsive real-time inspection of the automated fiber placement process. Int SAMPE Tech Conf 2020;2020-June. http://dx.doi.org/10.33599/s.20.0258.

[21] Nehls G. Fives introduces COAST in-process composite inspection technology. CompositesWorld 2023. URL https://www.compositesworld.com/products/fives-introduces-coast-in-process-composite-inspection-technology.

[22] Yadav N, Schledjewski R. Inline tape width control for thermoplastic automated tape layup. Composites A 2022;163. http://dx.doi.org/10.1016/J.COMPOSITESA.2022.107267.

[23] Peeters D, Quenzel P, Netzband L, Florindo AM, Hesseler S, Gries T. Predicting the formation of gaps and overlaps due to width variations of dry-fiber tapes during automated fiber placement. In: ACM5: fifth international symposium on automated composites manufacturing. 2022, URL https://www.ita.rwth-aachen.de/go/id/jfbg/file/844304.

[24] Tretiak I, Jones JL, Nguyen DH, Sun XC, Valverde MA, Kratz J. Real-time material measurement for automated fibre placement. In: Proceedings of the 20th European conference on composite materials - composites meet sustainability, vol. 2, European Society for Composite Materials; 2022, p. 25–31. http://dx.doi.org/10.5075/epfl-298799_978-2-9701614-0-0, European Conference on Composite Materials 2022: Composites meet sustainability, ECCM; Conference date: 26-06-2022 Through 30-06-2022. URL https://eccm20.org/.

[25] Ghayoor H, Shadmehri F, Van Hoa S. Development of experimental technique for measuring strain and deformation in manufacturing of thermoplastic composites using automated fiber placement (AFP). In: SAMPE 2014. Seattle, WA, 2014, URL https://www.researchgate.net/publication/286339438.

[26] Uhart M, Patrouix O, Aoustin Y, Canou J. Improving accuracy in robotized fiber placement. ICCM Int Conf Compos Mater 2013;2013-July:778–86.

[27] De Itzel Ojeda Jesus G, Patrouix O, Aoustin Y. Dynamic tool center point (DTCP) implementing in automated fiber placement (AFP). In: The third international symposium on automated composites manufacturing (ACM3). 2017, URL https://hal.science/hal-01509857.

[28] Jeffries KA. Enhanced robotic automated fiber placement with accurate robot technology and modular fiber placement head. SAE Int J Aerosp 2013;6(2):774–9. http://dx.doi.org/10.4271/2013-01-2290.

[29] Rudberg T. Increasing machine accuracy by spatially compensating large scale machines for use in constructing aerospace structures. SAE Int J Aerosp 2013;6(1):2013–01–2298. http://dx.doi.org/10.4271/2013-01-2298, URL https://www.sae.org/content/2013-01-2298/.

[30] Bock M, Perner M, Krombholz C, Beykirch B. Relation between repeatability and speed of robot-based systems for composite aircraft production through multilateration sensor system. In: Sensors and smart structures technologies for civil, mechanical, and aerospace systems 2015, vol. 9435, SPIE; 2015, p. 94352G. http://dx.doi.org/10.1117/12.2083846.

[31] Cheng L, Zhang L, Li J, Ke Y. Measurement, identification, and compensation of pose errors for six-axis gantry automated fiber placement machine. Int J Adv Manuf Technol 2022;120(3–4):2259–76. http://dx.doi.org/10.1007/s00170-021-08373-9.

[32] Xu X, Cheng L, Guo Y, Li J, Ke Y. A modeling and calibration method of heavy-duty automated fiber placement robot considering compliance and joint-dependent errors. J Mech Robotics 2023;15(6):61011–2. http://dx.doi.org/10.1115/1.4056405, URL https://asmedigitalcollection.asme.org/mechanismsrobotics/article/15/6/061011/1152261/A-Modeling-and-Calibration-Method-of-Heavy-Duty.

[33] ADDComposites. ADD Composites (Espoo, Finland) website. URL https://www.addcomposites.com/afpxs.

[34] Hexagon. Laser Tracker Fundamentals (11400-00-00). URL https://learning.hexagonmi.com/catalog/course.asp?id=16921&cid=6322.

[35] Hexagon AB. Leica Absolute Tracker AT960. URL https://hexagon.com/products/leica-absolute-tracker-at960.

[36] Ximea. Ximea xiC camera. URL https://www.ximea.com/en/products/usb-31-gen-1-with-sony-cmos-xic.

[37] Nguyen DH, Sun X, Tretiak I, Valverde MA, Kratz J. Automatic process control of an automated fibre placement machine. Composites A 2023;168:107465. http://dx.doi.org/10.1016/J.COMPOSITESA.2023.107465.

[38] Micro-Epsilon Messtechnik GmbH & Co KG. scanCONTROL 30x0. URL https://www.micro-epsilon.com/2D_3D/laser-scanner/scanCONTROL-3000/.

[39] Pantoji S, Kassapoglou C, Peeters D. Measuring sources of manufacturing process variations in automated fiber placement composites. In: Twenty-third international conference on composite materials (ICCM23). Belfast, Ireland; 2023, URL https://www.iccm-central.org/Proceedings/ICCM23proceedings/.

[40] King D. Automated fibre placement of Ox-Ox CMCs. In: 23rd international conference on composite materials. 2023, URL https://www.iccm-central.org/Proceedings/ICCM23proceedings/index.htm.